ChemComm

Spatial Arrangement of Dynamic Surface Species from Solid-State NMR and Machine Learning-Accelerated MD Simulations

Journal:	*ChemComm*
Manuscript ID	CC-COM-10-2022-005861.R1
Article Type:	Communication

COMMUNICATION

Spatial Arrangement of Dynamic Surface Species from Solid-State NMR and Machine Learning-Accelerated MD Simulations

Received 00th January 20xx,
Accepted 00th January 20xx

DOI: 10.1039/x0xx00000x

Takeshi Kobayashi,[a*] Da-Jiang Liu,[a*] and Frédéric A. Perras[a]

The surface arrangement of motional organic functionalities is explored by experimental dipolar coupling measurements and the prediction of motionally-averaged coupling constant from molecular dynamics simulations. The use of machine learning potentials was key to reaching the timescale required. The distance between dynamic surface species are important in cooperative heterogeneous catalysis.

NMR measurements of internuclear distances, which rely on the quantification of dipolar couplings, provide valuable constraints for determining the conformations of molecules and their arrangements. They are particularly valuable in materials that lack long-range order and thus cannot be studied using diffraction-based methods.[1-18] A well-known caveat, however, is that molecular motions have significant impacts on NMR-based distance measurements; for instance, SSNMR consistently overestimates bonded internuclear distances, when compared to single-crystal X-ray and neutron diffraction due to the librations and vibrations of the molecule.[19] Molecular motions that alter the internuclear vector direction, in particular, tend to dramatically reduce the magnitude of dipolar couplings, resulting in gross overestimations of internuclear distances. Common examples include methyl-rotation, which reduces ^{13}C–^{1}H dipolar couplings to only 1/3 their original size,[20, 21] and polymer chain dynamics which weaken ^{1}H–^{1}H dipolar couplings.[22]

The dynamics of organic and organometallic species tethered to silica materials have been studied using ^{2}H NMR spectroscopy in addition to dipolar-based methods,[23-31] often showing that surface species feature a high degrees of mobility. With general interest in developing methods to determine inter-site distances on surfaces and gain insights into cooperativity and isolation, it is necessary to find ways to recover accurate inter-site distances from NMR-based approaches.[15, 32-35]

One potential approach for the accurate measurement of internuclear distances using NMR spectroscopy is the application of molecular dynamics (MD) simulations to analyze molecular motions and estimate their impacts on dipolar couplings, as originally introduced by Ishii et al.[19] In the context of surface species, Paterson et al. combined dipolar coupling measurement and applied direct density functional theory (DFT) MD simulations to gain insights into the dynamics of grafted metal complexes.[36] While their approach was only partly successful in explaining the observed motions, this combination of accurate DFT MD methods for calculating dynamically-averaged dipolar coupling constants may well enable the use of NMR to analyze the structure and arrangement of mobile molecules on solid surfaces.

Herein, we apply a combination of MD simulations and ^{1}H–^{1}H distance measurements to explore the arrangement of allyl groups tethered to mesoporous silica nanoparticles (AL-MSNs).[37] To counter the reorientational dynamics of the allyl groups,[28] MD simulations need to cover timescales in excess of picoseconds to microseconds.[38, 39] Targeting such long timescales using DFT-based MD simulations is typically only achievable in very small systems. Recent advances in artificial intelligence have enabled the derivation of far less demanding force fields using DFT calculations and a machine learning (ML) approach. In this work, we used the DeePMD framework[40] and related software.[41]

The proximity of functional groups was first probed using a 2D ^{1}H double quantum / single-quantum (DQ/SQ) correlation experiment using the BABA recoupling sequence.[42] This experiment only generates correlation signals for pairs of nuclear spins. In the DQ/SQ spectrum of AL-MSN (Fig. 1), correlations were observed between all possible intramolecular spin pairs, but, more importantly, we observe an H2–H2 correlation that can only be explained by an intermolecular

[a] U.S. DOE Ames National Laboratory, Ames, IA, 50011, USA.

† Electronic Supplementary Information (ESI) available: See DOI: 10.1039/x0xx00000x

contact between proximate functional groups (see Fig. 1 for assignments).

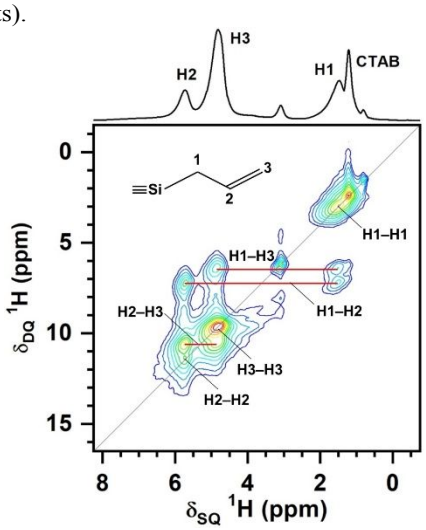

Fig. 1 Rotor-synchronized ^{1}H DQ/SQ correlation spectrum of AL-MSN. A τ_{rec} of 160 μs was used. The 2D spectrum was acquired on a Varian VNMRS 600 MHz spectrometer equipped with a 1.6 mm MAS probe, a 25 kHz MAS frequency, 320 t_1 increment of 40 μs, 32 scans, and a recycle delay of 0.8 s.

In ideal circumstances, it may be possible to determine the magnitude of dipolar couplings by measuring the build-up of the DQ coherences,[43] but a more reliable approach is to analyze the MAS sideband patterns in the DQ dimension.[11, 44-46] For the latter experiment, a 2D DQ/SQ correlation spectrum is recorded, with a non-rotor-synchronized t_1 increment, such that the rotor has different orientations at the beginning of the excitation and reconversion periods. Consequently, the phase at reconversion is shifted with respect to the phase of excitation and the reconversion becomes rotor-encoded, thus generating spinning sidebands. The spinning sideband patterns are dependent of the DQ excitation times; generally recoupling times (τ_{rec}) where $D_{ij} \times \tau_{rec}/2\pi = 0.5 \sim 1$ are sufficient for the measurement of distances ($D_{i,j}$ is the dipolar coupling constant). [45]

With 120 μs of DQ recoupling time, the H1–H1 and H3–H3 correlation peaks showed the expected odd-ordered DQ sidebands (Fig. 2b and c, respectively). The negligible even-ordered DQ sidebands and centerband indicate that the DQ coherence involves relatively isolated spin pairs.[44, 45] By fitting the recorded DQ sideband patterns using SIMPSON,[47] the dipolar couplings were estimated to be 11.6 kHz for the H1–H1 pair (blue line in Fig. 2b) and 6.6 kHz for the H3–H3 pair (green in Fig. 2c). Motions also lead to the appearance of a non-zero dipolar asymmetry, a fact that was included in the simulations through the incorporation of a dipolar asymmetry parameter η_D. Ignoring this effect leads to a slightly larger H1-H1 dipolar coupling constant (13.3 kHz), while it did not significantly affect the estimation of the other dipolar coupling strengths (see Fig. S3 in ESI for more details). Third-spin effects on the sideband manifolds were also found to be negligible (see Fig. S4 in ESI). The expected H1-H1 and H3-H3 distances are 0.181 and 0.187 nm, respectively, corresponding dipolar coupling constants of 20 and 18 kHz. As such, the dynamics of the AL groups are well evidenced by the low order parameters ($\langle S \rangle = \langle D \rangle / D$) of 0.67 and 0.37 for the H1 and H3 sites, respectively. The lower $\langle S \rangle$ value measured for the H3-H3 pair agrees with the fact that this site is located farther from the surface and experiences composite rotations, consistent with observations made on other functional groups.[28]

To observe DQ sidebands from the H2–H2 correlation it was necessary to perform an experiment with a longer recoupling time of 320 μs (Fig. 2d). The observed sideband pattern (Fig. 2e) could be simulated using an effective H2–H2 dipolar coupling of 1.3 kHz; however, without knowing, $\langle S \rangle$, the H2–H2 internuclear distance cannot be determined.[19]

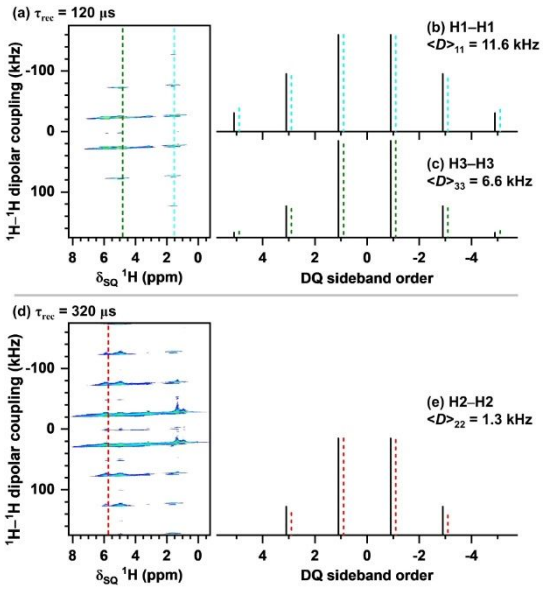

Fig. 2 Non-rotor-synchronized ^{1}H DQ/SQ correlation spectra of AL-MSN (a, d), and the resulting DQ sideband patterns for the self-correlation peaks (b, c, and e). Solid and dashed lines represent the best-fit simulations and the experimentally obtained spinning sidebands. Simulated spectra are shown in black. τ_{rec} was set to 120 μs (a-c) or 320 μs (d, e). The 2D spectra were acquired under 25 kHz MAS in 3200 t_1 increment of 2.5 μs, 64 scans, and a recycle delay of 0.8 s.

To reproduce the ^{1}H–^{1}H dipolar couplings observed experimentally, we applied DeePMD simulations to multiple models either based on the surfaces reported by Comas-Vives,[48] or created from β-cristobalite.[49-51] Force fields were derived using a training data set consists of 141 individual DFT MD simulations, with each run consisting of 2000 times steps, with time step ranges from 0.5 to 5 fs, depending on the lightest element in the simulation. DFT MD simulations were performed using VASP (v5.4), with the PBE functional and recommended[52, 53] projector augmented wave (PAW) potentials.[54] Kinetic energy cutoffs of 400 eV were used for all elements with a 0.2 eV Gaussian smearing of the electron occupancy. More details of the methodology can be found elsewhere.[55]

Given that the majority of T^n sites ($(\equiv SiO–)_n\mathbf{Si}R(–OH)_{3-n}$, n = 1, 2, 3) are connected to another T^n site through a siloxane bridge, or at an otherwise close distance to one,[32, 34] models were created that incorporated two allyl groups on adjacent silica sites. These were built by either replacing the silanol hydroxyl group or a siloxane oxygen with the allyl moiety. Any resulting 3-coordinate Si sites were terminated by a hydroxyl group.

Models were then optimized with damped MD for 1 ps using the DeePMD potential. After this, a sequence of 10 ps, 100 ps, and 1 ns DeePMD simulations at 300 K were performed using the ASE package.[56] Atomic trajectories were stored every 10 fs. The motionally-averaged intra- and intermolecular ^{1}H–^{1}H dipolar couplings were calculated by extending the method introduced by Paterson et al.[36] to take into account the variations in internuclear distances. Briefly, we calculate the lab frame Cartesian dipolar coupling tensor ($\mathbf{D}_{\mathrm{LAB}}$) at each time step (i) and calculate a rolling average of the tensor ($\langle\mathbf{D}\rangle$, eqn. 1). $\langle\mathbf{D}\rangle$ is then diagonalized to determine the dynamically averaged dipolar coupling constant $\langle D\rangle$ and the asymmetry of the tensor. By plotting $\langle D\rangle$ as a function of the simulation time, we can follow its convergence and determine its steady-state value.

$$\langle\mathbf{D}\rangle = \frac{1}{N}\sum_{\mathrm{i}=1}^{N}\mathbf{D}_{\mathrm{LAB,\,i}} \qquad (1)$$

Five separate models with the two AL moieties situated at different locations on the SiO_2 surface were simulated. Fig. 3a shows the results obtained on one of these models which was in best agreement with the experiment. Fig. 3b shows the evolutions of computed $\langle D\rangle$ values as a function of the MD simulation time. In this model, neither AL group experience steric interactions with the surface, allowing them to move freely. These motions result in significant motional averaging of H1–H1 and H3–H3 intramolecular dipolar couplings to 14.1 kHz and 6.3 kHz, respectively, which are close to those measured experimentally (11.6 kHz and 6.6 kHz). Interestingly, the predicted H2–H2 dipolar coupling appears to be an accurate measure of the average distance between the two sites. For instance, the simulation yielded an average H2-H2 distance of 0.46 nm and a corresponding $\langle D\rangle$ value of 1.1 kHz. 1.1 kHz would equate to a static ^{1}H–^{1}H distance of 0.48 nm, 0.02 nm from the average value. We suspect that the losses in coupling from orientational changes were counterbalanced by the $\langle d^{-3}\rangle$ averaging emphasizing the brief moments when the H2–H2 distance is shorter than the average. Intramolecular H1–H2 and H2–H3 dipolar couplings were extensively motionally averaged to ~2 kHz in the simulations.

The four other models successfully reproduced the reduction in the intramolecular H1–H1 and H3–H3 dipolar couplings but not the intermolecular H2–H2 dipolar coupling, which tended to be in the range of 350-550 Hz (see Fig. S1 in ESI). We suspect that the double-quantum filtering in the experiment selects for the closest spin pairs, giving us a view of the nearest AL-AL neighbors but not the average AL-AL distance. This is corroborated by the lower amplitude of the H2-H2 correlation in the DQ/SQ spectrum (Fig. 1).

The structure shown in Fig. 3a is the lowest energy structure from the DeePMD simulation at 300 K, further DFT-optimized at 0 K. In this 0 K structure the H2–H2 distance increases to 0.65 nm, which is considerably longer than the average H2–H2 distance of 0.46 nm. This result shows that ground state structures may fall prey to local potential energy minima that may not be representative of the true, dynamic, structure. Histograms of the H2-H2 distance, and the orientations of all three H-H vectors from the DeePMD simulation are given in Fig. 4b-g. Orientations are described using polar angles θ and ϕ (see Fig. 4). The presence of multiple peaks in the histograms indicates that the system jumps between local energy minima and accordingly suggests that: 1) the structure is temperature-dependent and 2) the energy landscape sampled by the simulation requires sufficient time to overcome the energy barriers to move between conformers (see also Fig. S2 in ESI).

At simulation times below 100 ps, a practical limit for direct DFT MD simulations of amorphous silica systems,[36] none of the motionally-averaged dipolar couplings in Fig. 3b had converged. After 1 ns of simulation, however, all three dipole couplings are in reasonable agreement with experiment. Ideally, we would want to average for tens of microseconds, the timescale of the interaction, but such timescales are still beyond reach for this level of theory.

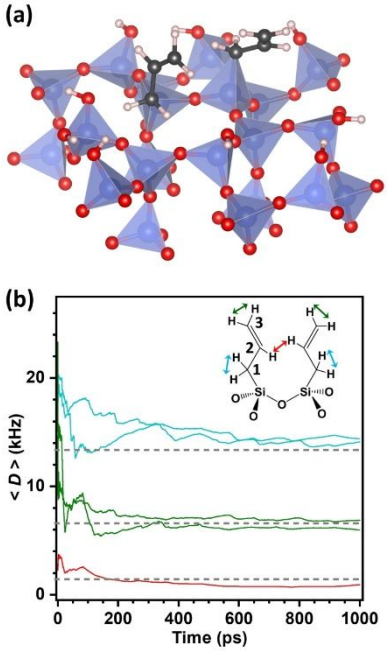

Fig.3 Model of the AL groups on the silica surface (a), and the evolution of ^{1}H–^{1}H dipolar coupling as a function of the DeePMD simulation time (b). In (a), purple tetrahedra represents SiO_4. Red, white, and grey spheres represent oxygen, hydrogen, and carbon atoms, respectively. Not all atoms used for the MD simulations are shown. In (b), the grey dashed lines represent the experimental dipolar coupling values.

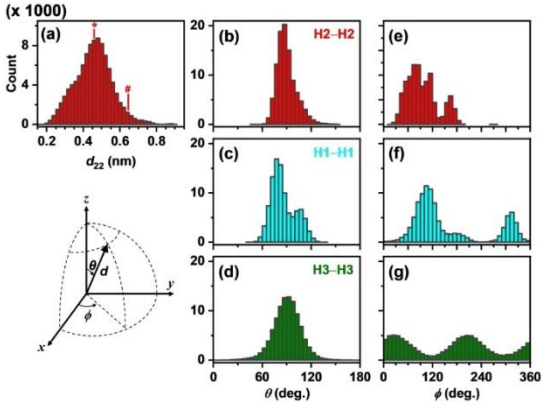

Fig. 4. Histograms of d_{22} (a), θ (b-d), and ϕ (e-g) observed during the DeePMD simulation from Fig. 3a. In (a), an asterisk indicates the average d_{22} value, while a number sign indicates the d_{22} value in the lowest energy structure.

In summary, we studied the arrangement of mobile organic functionalities tethered to mesoporous silica using intermolecular ^{1}H-^{1}H distance measurements. Analysis of the data required an accurate treatment of the molecular motions, and how they average dipolar coupling tensors. This was achieved using a machine learning-accelerated MD simulation of periodic functionalized silica surface models. Due to the presence of local energy minima, relatively long simulation times are required to estimate motionally averaged dipolar interactions, and as such the implementation of the machine learning algorithm was key to the success of the simulations. Good agreement was obtained with one structure for which inter-functional group steric interactions were minimized and the two groups were able to maintain a short average distance. We expect that the DQ-filtering of the experiment is biased towards the detection of such pairs. Importantly, the dynamically-averaged intermolecular dipolar coupling constants were found to be representative of the average internuclear distance. This combination of solid-state NMR and a machine learning-accelerated MD can be a practical tool for studying the arrangements of mobile species on surfaces and cooperativity between sites, particularly in systems where conventional MD simulations are cost-prohibitive.

This research is supported by the U.S. Department of Energy, Basic Energy Sciences, Division of Chemical Sciences, Geosciences, and Biosciences through the Ames Laboratory. Molecular dynamics calculations (DJL) were supported by the Computational and Theoretical Chemistry (CTC) project. The analysis of the dynamic data was supported by a DOE Early Career Research Project (FAP). Ames National Laboratory is operated for the DOE by Iowa State University under Contract No. DE-AC02-07CH11358.

Conflicts of interest

There are no conflicts to declare.

Notes and references

1 W. Braun, C. Bosch, L. R. Brown, N. Go, K. Wuthrich, *Biochim. Biophys. Acta*, 1981, **667**, 377.
2 H. W. Spiess, *Chem. Rev.*, 1991, **91**, 1321.
3 T. Yamamura, T. Watanabe, A. Kikuchi, M. Ushiyama, T. Kobayashi, H. Hirota, *J. Phys. Chem.*, 1995, **99**, 17062.
4 K. Schmidt-Rohr, *Macromol.*, 1996, **29**, 3975.
5 R. G. Griffin, *Nat. Struct. Biol.*, 1998, **5**, 508.
6 Y. Ishii, *J. Chem. Phys.*, 2001, **114**, 8473.
7 M. Baldus, *Prog. Nucl. Magn. Reson. Spectrosc.*, 2002, **41**, 1.
8 R. Tycko, *Curr. Opin. Struct. Biol.*, 2004, **14**, 96.
9 Z. H. Gan, *Chem. Commun.*, 2006, 4712.
10 G. De Paepe, J. R. Lewandowski, A. Loquet, A. Bockmann, R. G. Griffin, *J. Chem. Phys.*, 2008, **129**, 245101.
11 M. R. Hansen, R. Graf, S. Sekharan, D. Sebastiani, *J. Am. Chem. Soc.*, 2009, **131**, 5251.
12 B. Hu, O. Lafon, J. Trebosc, Q. Chen, J.-P. Amoureux, *J. Magn. Reson.*, 2011, **212**, 320.
13 X. Q. Kong, H. X. Deng, F. Y. Yan, J. Kim, J. A. Swisher, B. Smit, O. M. Yaghi, J. A. Reimer, *Science*, 2013, **341**, 882.
14 E. Nimerovsky, R. Gupta, J. Yehl, M. Y. Li, T. Polenova, A. Goldbourt, *J. Magn. Reson.*, 2014, **244**, 107.
15 T. Kobayashi, I. I. Slowing, M. Pruski, *J. Phys. Chem. C*, 2017, **121**, 24687.
16 P. Berruyer, M. Lelli, M. P. Conley, D. L. Silverio, C. M. Widdifield, G. Siddiqi, D. Gajan, A. Lesage, C. Coperet, L. Emsley, *J. Am. Chem. Soc.*, 2017, **139**, 849.
17 F. A. Perras, J. D. Padmos, R. L. Johnson, L. L. Wang, T. J. Schwartz, T. Kobayashi, J. H. Horton, J. A. Dumesic, B. H. Shanks, D. D. Johnson, et al., *J. Am. Chem. Soc.*, 2017, **139**, 2702.
18 D. Nghia Tuan, S. Raran-Kurussi, Y. Nishiyama, V. Agarwal, *J. Phys. Chem. Lett.*, 2018, **9**, 5948.
19 Y. Ishii, T. Terao, S. Hayashi, *J. Chem. Phys.*, 1997, **107**, 2760.
20 Y. J. Lee, T. Murakhtina, D. Sebastiani, H. W. Spiess, *J. Am. Chem. Soc.*, 2007, **129**, 12406.
21 J. J. Kinnun, A. Leftin, M. F. Brown, *J. Chem. Educ.*, 2013, **90**, 123.
22 K. Saalwachter, P. Ziegler, O. Spyckerelle, B. Haidar, A. Vidal, J. U. Sommer, *J. Chem. Phys.*, 2003, **119**, 3468.
23 B. Boddenberg, R. Grosse, U. Breuninger, *Surf. Sci.*, 1986, **173**, L655.
24 F. Blanc, J. M. Basset, C. Coperet, A. Sinha, Z. J. Tonzetich, R. R. Schrock, X. Solans-Monfort, E. Clot, O. Eisenstein, A. Lesage, et al., *J. Am. Chem. Soc.*, 2008, **130**, 5886.
25 T. Kobayashi, J. A. DiVerdi, G. E. Maciel, *J. Phys. Chem. C*, 2008, **112**, 4315.
26 J. Gath, G. L. Hoaston, R. L. Vold, R. Berthoud, C. Coperet, M. Grellier, S. Sabo-Etienne, A. Lesage, L. Emsley, *Phys. Chem. Chem. Phys.*, 2009, **11**, 6962.
27 Q. Q. Wang, E. Jordan, D. F. Shantz, *J. Phys. Chem. C*, 2009, **113**, 18142.
28 S. Nedd, T. Kobayashi, C. H. Tsai, I. I. Slowing, M. Pruski, M. S. Gordon, *J. Phys. Chem. C*, 2011, **115**, 16333.
29 S. Jayanthi, V. Frydman, S. Vega, *J. Phys. Chem. B*, 2012, **116**, 10398.
30 M. Weigler, M. Brodrecht, H. Breitzke, F. Dietrich, M. Sattig, G. Buntkowsky, M. Vogel, *Z. Phys. Chem.*, 2018, **232**, 1041.
31 E. Steinrucken, T. Wissel, M. Brodrecht, H. Breitzke, J. Regentin, G. Buntkowsky, M. Vogel, *J. Chem. Phys.*, 2021, **154**, 114702.
32 T. Kobayashi, D. Singappuli-Arachchige, Z. R. Wang, I. I. Slowing, M. Pruski, *Phys. Chem. Chem. Phys.*, 2017, **19**, 1781.
33 T. Kobayashi, D. Singappuli-Arachchige, I. I. Slowing, M. Pruski, *Phys. Chem. Chem. Phys.*, 2018, **20**, 22203.
34 T. Kobayashi, M. Pruski, *ACS Catal.*, 2019, **9**, 7238.
35 R. Jabbour, M. Renom-Carrasco, K. W. Chan, L. Volker, P. Berruyer, Z. R. Wang, C. M. Widdifield, M. Lelli, D. Gajan, C. Coperet, et al., *J. Am. Chem. Soc.*, 2022, **144**, 10270.
36 A. L. Paterson, D. J. Liu, U. Kanbur, A. D. Sadow, F. A. Perras, *Inorg. Chem. Front.*, 2021, **8**, 1416.
37 S. Huh, J. W. Wiench, J. C. Yoo, M. Pruski, V. S. Y. Lin, *Chem. Mater.*, 2003, **15**, 4247.
38 D. J. Cerasale, D. C. Ward, T. L. Easun, *Nat. Rev. Chem.*, 2021, **6**, 9.
39 M. Seifrid, G. N. M. Reddy, B. F. Chmelka, G. C. Bazan, *Nat. Rev. Mater.*, 2020, **5**, 910.
40 L. F. Zhang, J. Q. Han, H. Wang, R. Car, E. Weinan, *Phys. Rev. Lett.*, 2018, **120**, 143001.
41 H. Wang, L. F. Zhang, J. Q. Han, W. N. E, *Comput. Phys. Commun.*, 2018, **228**, 178.
42 M. Feike, D. E. Demco, R. Graf, J. Gottwald, S. Hafner, H. W. Spiess, *J. Magn. Reson. A*, 1996, **122**, 214.
43 M. J. Bayro, M. Huber, R. Ramachandran, T. C. Davenport, B. H. Meier, M. Ernst, R. G. Griffin, *J. Chem. Phys.*, 2009, **130**, 114506.
44 I. Schnell, H. W. Spiess, *J. Magn. Reson.*, 2001, **151**, 153.
45 I. Schnell, A. Watts, H. W. Spiess, *J. Magn. Reson.*, 2001, **149**, 90.
46 K. Saalwachter, *ChemPhyschem*, 2013, **14**, 3000.
47 Z. Tosner, R. Andersen, B. Stevenss, M. Eden, N. C. Nielsen, T. Vosegaard, *J. Magn. Reson.*, 2014, **246**, 79.
48 A. Comas-Vives, *Phys. Chem. Chem. Phys.*, 2016, **18**, 7475.
49 D. R. Peacor, *Z. Kristallogr.*, 1973, **138**, 274.
50 J. S. Beck, J. C. Vartuli, W. J. Roth, M. E. Leonowicz, C. T. Kresge, K. D. Schmitt, C. T. W. Chu, D. H. Olson, E. W. Sheppard, S. B. McCullen, et al., *J. Am. Chem. Soc.*, 1992, **114**, 10834.
51 K. J. Edler, P. A. Reynolds, J. W. White, *J. Phys. Chem. B*, 1998, **102**, 3676.
52 G. Kresse, J. Hafner, *Phys. Rev. B*, 1994, **49**, 14251.
53 VASP - Vienna Ab initio Simulation Package, <https://www.vasp.at/>.
54 G. Kresse, D. Joubert, *Phys. Rev. B*, 1999, **59**, 1758.
55 D. J. Liu, J. W. Evans, *J. Chem. Phys.*, 2022, **156**, 204106.
56 A. H. Larsen, J. J. Mortensen, J. Blomqvist, I. E. Castelli, R. Christensen, M.

Dulak, J. Friis, M. N. Groves, B. Hammer, C. Hargus, et al., *J. Phys. Condens. Matter*, 2017, **29**, 273002.